aerospace

MDPI

Article

Combustion Characteristics of HTPB-Based Hybrid Rocket Fuels: Using Nickel Oxide as the Polymer Matrix Pyrolysis Catalyst

Hongsheng Yu [1,2], Xiaodong Yu [1,2], Hongwei Gao [1,2], Luigi T. DeLuca [1,3], Wei Zhang [1,2,*] and Ruiqi Shen [1,2,*]

[1] Institute of Space Propulsion, Nanjing University of Science and Technology, Nanjing 210094, China; hongshengyu2017@foxmail.com (H.Y.)
[2] Micro-Nano Energetic Devices Key Laboratory of MIIT, Nanjing 210094, China
[3] Space Propulsion Laboratory (SPLab), Department of Aerospace Science and Technology, Politecnico di Milano, 20156 Milan, Italy
* Correspondence: wzhang@njust.edu.cn (W.Z.); rqshen@njust.edu.cn (R.S.)

Abstract: The slow regression rate induced by the high pyrolysis difficulty has limited the application and development of hydroxyl-terminated polybutadiene (HTPB)-based fuels in hybrid rocket propulsion. Nickel oxide (NiO) shows the possibility of increasing the regression rate of HTPB-based fuels by catalyzing the pyrolysis process of the polymer matrix in our previous investigation; hence, this paper studies the NiO particles in the thermal decomposition and combustion of HTPB fuel grains. The DSC/TG test shows that NiO can intensely decrease the thermal stability of HTPB, and the catalytic effect of NiO is mainly reflected in the final decomposition stages of polybutadiene components. 5 wt% NiO enhances the regression rate by 19.4% and 13.7% under an oxygen mass flux of 50 kg/m^{2}s and 150 kg/m^{2}s, respectively. Further investigation shows that NiO particles will also cause the reduction of combustion heat and the agglomeration at the regressing surface while catalyzing the pyrolysis process, improving the thermal conductivity, and promoting the radiative heat transfer of the HTPB-based fuels; thus, more NiO additive (5 wt% < [NiO] $\leq$ 10 wt%) does not lead to a faster regression rate in HTPB-based fuels. This study demonstrates the catalytic effect of NiO on the polymer matrix for HTPB-based fuels, showing the attractive application prospects of this additive in HTPB-containing fuel grains.

Keywords: hybrid rocket propulsion; HTPB; combustion characteristics; regression rate; catalytic pyrolysis; nickel oxide

Citation: Yu, H.; Yu, X.; Gao, H.; DeLuca, L.T.; Zhang, W.; Shen, R. Combustion Characteristics of HTPB-Based Hybrid Rocket Fuels: Using Nickel Oxide as the Polymer Matrix Pyrolysis Catalyst. *Aerospace* **2023**, *10*, 800. https://doi.org/10.3390/aerospace10090800

Academic Editor: Jae Hyun Park

Received: 30 June 2023
Revised: 21 August 2023
Accepted: 24 August 2023
Published: 13 September 2023

1. Introduction

Hybrid rocket propulsion is wisely investigated for its safety, reliability, environment friendliness, and low cost, hence regarded as a promising candidate in suborbital flight, space tourism, and small satellite orbital injection [1–7]. Resulting from their superior mechanical properties, the hydroxyl-terminated polybutadiene (HTPB)-based fuels are extensively investigated polymer matrix in hybrid rocket propulsion [1,8–11]. Nevertheless, the slow regression rate induced by the high pyrolysis difficulty has limited the application and development of HTPB-based fuels [2,12]. The traditional methods of overcoming this intrinsic limit, such as adding high calorific value metal powder, introducing energetic materials or solid oxidizer, porous engine charge, using liquefied fuels such as paraffin, and oxidizer vortex injection can effectively increase the regression rate of fuel grains, but also lead to agglomeration, reduced safety, reduced charge, poor fuel mechanical properties, and increased engine structural complexity [13–26].

Lots of scientific works found in the literature have proved that some transition metal elements can catalyze thermal decomposition and even promote the burning process of the

polymer. Varfolomeev et al. found that copper stearate can accelerate the oxidation process of crude oil and shift both the low-temperature oxidation (LTO) and high-temperature oxidation (HTO) to lower temperatures [27]; Moroi reported that manganese, cobalt, iron, chromium, and copper metal ions decrease the thermal stability and promote the thermal degradation of the polyesterurethane [28]; Pal et al. indicated that 10 wt% cerium oxide reduces the activation energy of pure paraffin from 254 kJ/mol to 222 kJ/mol, hence leading to a notable regression rate increase [29]. As for HTPB-based fuels, appropriate catalysts can reduce the thermal decomposition temperature, accelerate the pyrolysis process, and thereby increase the regression rate of the fuel grains. There are only a few studies using acetylacetone complexes as the pyrolysis catalyst to improve the regression rate that have been published. Cardoso et al. revealed that acetylacetone complexes accelerate the pyrolysis of HTPB-based fuels at high temperatures, and 7.62 wt% copper acetylacetone enhances the regression rate of a 40 paraffin particles/60 HTPB composite by 82.2% at oxygen mass flux (G_{ox}) = 5 kg/m^{2}s [30]; Yu et al. demonstrated that acetylacetone complexes can decrease the thermal stability of the HTPB matrix, and the catalytic effect of nickel acetylacetonate on HTPB is mainly induced by the Ni^{2+} at the early stage of decomposition, and by the produced NiO in the final degradation stage, which corresponds to the decomposition of the polybutadiene component [31,32].

Since NiO shows the ability to catalyze the decomposition of the polybutadiene component, which dominates the burning process of HTPB fuel grains, in this paper, the NiO is used to promote the regression rate of HTPB-based fuels by accelerating the pyrolysis of the polymer matrix. The prepared pure HTPB and NiO-loaded fuels, coordinating with several characterization methods including thermal test, combustion test, and morphological characterization, were used to reveal the catalytic effect and mechanism of NiO on HTPB-based fuels.

2. Experiment

2.1. Materials

The HTPB (CAS: 69102-90-5) pre-polymer with an average molecular weight of 2872 g/mol and -OH content of 0.7747 mmol/g was obtained from Zibo Qilong Chemical Co., Ltd., Zibo, China; the isophorone diisocyanate (IPDI, CAS: 4098-71-9) curing agent, dibutyltin diacetate (TIN, CAS: 77-58-7) curing catalyst, and dioctyl adipate (DOA, CAS: 123-79-5) plasticizer were purchased from Shanghai Aladdin Biochemical Technology Co., Ltd., Shanghai, China; the nickel oxide (NiO, CAS: 1313-99-1) was supplied by the MeryerBiochemical Technology Co., Ltd., Shanghai, China.

2.2. Fuel Preparation

The pure HTPB and 1.25 wt%, 2.50 wt%, 5.00 wt%, 7.50 wt%, and 10.0 wt% NiO-loaded fuels were prepared, where the pure HTPB was the baseline in this study. The detailed composition of all fuels can be seen in Table 1, and the R value ([-NCO]/[-OH]) is set to 1.05. Figure 1 shows the fabrication process of pure HTPB and the NiO-loaded formulations. A specific proportion of HTPB prepolymer, DOA, and TIN components were added to a 500 mL stirring cup, and the ZKJ-3 type vacuum mixer was used to vacuumize the stirring cup (<5 kPa) and mix the reactants at a constant speed of 270 rpm for 5 min. Following this step, the NiO powder was added to the vacuum stirring cup and mixed for 15 min. The IPDI curing agent was finally added to the slurry and treated in the same condition for 10 min. The uniformly stirred slurry was cast into several 19 mm OD × 16 mm ID × 30 mm length 304 steel pipe molds (equipped with a 4.5 mm OD PTFE center rod) in the atmosphere and solidified at 36 °C in an oven for 24 h followed by a 72 h post-cure bake at 60 °C.

Table 1. The composition of pure HTPB and NiO-loaded formulations.

Formulation	HTPB, wt%	DOA, wt%	IPDI, wt%	TIN, wt%	NiO, wt%
Pure HTPB	79.29	13.04	7.24	0.43	0
1.25% NiO	78.30	12.88	7.15	0.42	1.25
2.50% NiO	77.31	12.71	7.06	0.42	2.50
5.00% NiO	75.33	12.39	6.88	0.41	5.00
7.50% NiO	73.34	12.06	6.70	0.40	7.50
10.0% NiO	71.36	11.74	6.52	0.38	10.00

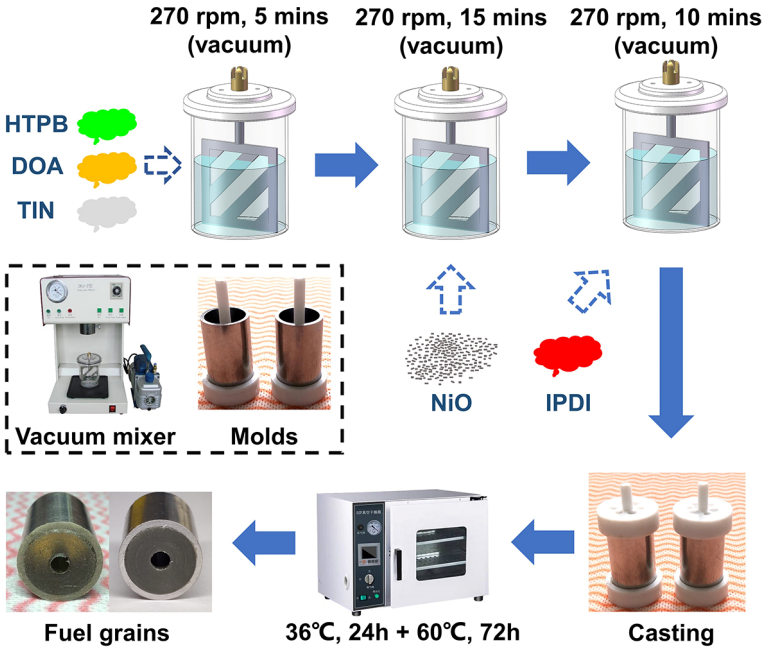

Figure 1. The fabrication process of the pure HTPB and NiO-loaded formulations.

2.3. Characterization Methods

The surface morphology of the used NiO particles and prepared HTPB-based fuels was characterized by field emission scanning electron microscopy (SEM, Quanta 250FEG) under 10.0 kV accelerating voltage. The energy dispersive spectrometer (EDS mapping) equipped in SEM was used to determine the element distribution of the fuel surface for prepared composites. A laser particle size analyzer (Malvern Mastersizer 2000) was adopted to investigate the particle size distribution of NiO particles. The simultaneous differential scanning calorimetry/thermal gravimetric (DSC/TG, Netzsch STA449C) was performed to clarify the thermal decomposition process of pure HTPB and NiO-loaded fuels under a heating rate of 10 K·min^{-1} with a 40 mL·min^{-1} air atmosphere. A hot disk thermal analyzer (Hot Disk TPS2500) equipped with a 6.40 mm radius Kapton sensor was used to characterize the thermal conductivity of all prepared fuels at 298 K.

2.4. Hybrid Propulsion Combustion System

As shown in Figure 2, a 2D-radial hybrid burner, based on the original design by the Space Propulsion Laboratory (SPLab) of Politecnico di Milano, was used to perform combustion tests on HTPB-based fuels [33]. An actual picture of the facility is presented in Figure S1 of the Supplementary Materials [31]. Gaseous oxygen, as the oxidizer in the combustion test, was axially injected into the grain port at a mass flow rate of 3 g/s. The oxidizer injector is designed to grant optical access to the tested specimen head-end, thus providing the possibility to track the central port diameter during the combustion. A feedback loop automatic system (based on PID algorithm) combined with solenoid valves and pressure transducer controlled chamber pressure granting a quasi-steady value of

1.0 MPa. B/KNO_3/phenolic resin (40/60/0.5 wt%) primer charge, with 4.5 mm OD × 1 mm thickness, was ignited by laser, providing a non-intrusive system for specimen ignition [34]. The burning process of the cross-section was recorded by a high-speed camera operating at 500 fps and 432 × 432 resolution. A scheme of the injector implementation and optical path for the visualization of the burning strand head-end is reported in Figure 2. Gaseous nitrogen was used to terminate the combustion before the complete consumption of the fuel. A time-resolved technique was used for the regression rate (r_f) determination. This data reduction procedure enables the identification of relevant ballistic parameters (including the oxidizer mass flux). Full details on the method are reported in our previous papers [19,35]. The pure HTPB is taken as the baseline for comparison and relative scoring of the tested formulations. Three to five combustion tests were performed for each formulation. Single test data were collapsed in an ensemble average curve enabling the definition of error bars based on standard deviation.

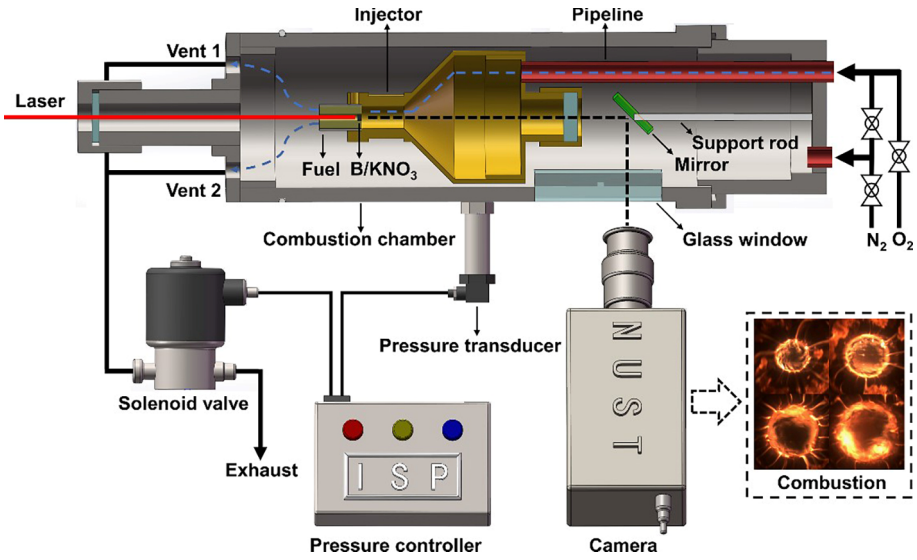

Figure 2. The schematic description of the 2D-radial hybrid burner [31].

3. Results and Discussion

Figure 3 shows the surface morphology of the NiO particles and the homogeneity of the cast fuel grains (the surface morphology of all NiO-loaded fuels is presented in Figure S2 of the Supplementary Materials). Figure 3e shows that the NiO particles have a uniform particle size distribution. The average particle size (D_{50}) measured by a laser particle size analyzer is 12.08 μm, while the SEM images show that NiO is equipped with a submicron size. The above difference in the test results originates from the too-small particle size of the NiO, which is prone to agglomerate and results in a larger particle size, finally measured by the laser particle size analyzer. The agglomeration of NiO particles can be confirmed by the SEM image of Figure 3e.

From the SEM images (in Figure 3) of the prepared HTPB-based fuels, the pure HTPB shows its homogeneity without cracks or pores, demonstrating the feasibility of the fuel preparation process (shown in Figure 1). The 1.25% NiO, 5.00% NiO, and 10.0% NiO formulations were selected to exhibit the homogeneity of the NiO-loaded fuels. In the SEM image with a scale of 250 μm, the NiO particles are evenly distributed in the HTPB-based fuels. While the scale is enlarged to 10 μm, the NiO particles agglomerated in the NiO-loaded fuels, and this phenomenon deteriorated with the increase in the NiO content. The EDS mapping images of the NiO-loaded fuels clearly show the agglomeration of the NiO particles in the HTPB matrix, which is consistent with the results in Figure 3e. Especially for 10.0% NiO, even large NiO balls appear in the fuel grains.

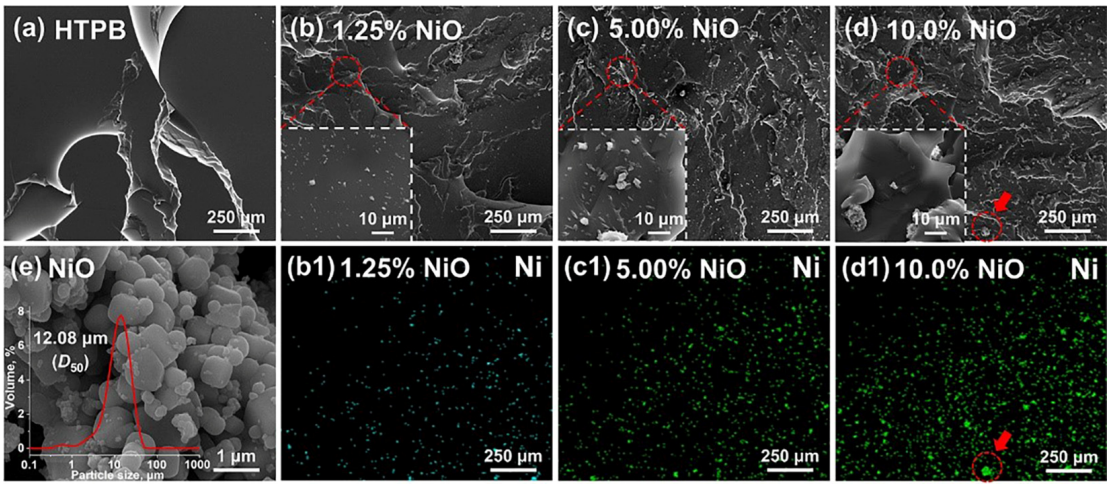

Figure 3. The surface morphology of the NiO particles and prepared HTPB-based fuels. (**a**–**d**) SEM images of the pure HTPB and NiO-loaded fuels; (**b1**–**d1**) EDS mapping images of the NiO-loaded fuels; (**e**) SEM and particle size distribution images of the NiO particles.

To reveal the effects of NiO particles on the pyrolysis process of the HTPB matrix, Figure 4 shows the TG-DSC curves of the pure HTPB and NiO-loaded fuels. The experimental results show that NiO mainly affects the thermal decomposition process of the polybutadiene component, which dominates the pyrolysis and combustion process of the HTPB-based fuels. NiO causes splitting and shifting of the exothermic peaks (T_1 and T_2) of polybutadiene components, while these effects are slight from an overall point of view. The above experimental results show that NiO particles have a weak effect on the early- and mid-term thermal decomposition of polybutadiene components, and basically no catalytic effect is shown. With the increase of NiO content, the end temperature (T_{End}) of NiO-loaded fuels significantly decreases from 615 °C (pure HTPB) to 573 °C (10.0% NiO). Combined with the weak change of the peak temperature of the prepared fuels at T_1 and T_2, the experimental results show that the catalytic effect of NiO on the polybutadiene component is mainly reflected in the late-term thermal decomposition process, that is, the end of the thermal decomposition process of the HTPB-based fuels. Figure 5 shows the end temperature difference between pure HTPB and NiO-loaded fuels. When the NiO content is lower than 5 wt%, the end temperature of the HTPB-based fuels decreased rapidly with the increasing NiO. Starting from 5 wt% of NiO, the NiO-loaded fuels show a slow decrease in the end temperature relative to the pure HTPB fuel. The experimental results indicate that when the content of NiO particles is lower than ($\leq$) 5 wt%, its catalytic pyrolysis effect on HTPB-based fuels will be significantly enhanced with the increase of NiO content, followed by (>5 wt%) the decrease of the benefit–cost ratio for the catalytic effect. The TG test shows that the NiO particles also lead to a significant increase in residue content during the pyrolysis process of the HTPB-based fuels.

To further investigate the effect of NiO particles on the combustion performance of HTPB-based fuels, Figure 6 illustrates the thermal conductivity of the pure HTPB and NiO-loaded fuels, and the specific values are shown in Table S1 of the Supplementary Materials. NiO increases the thermal conductivity of HTPB-based fuels, while the NiO-loaded fuels show a slow increase in the thermal conductivity once the NiO content exceeds 2.50 wt%. It should also be noted that NiO does not exhibit a significant increase in thermal conductivity for HTPB-based fuels. Even for the 10.0% NiO which provides the highest thermal conductivity, the thermal conductivity is only increased by 6.61% compared to the pure HTPB fuel.

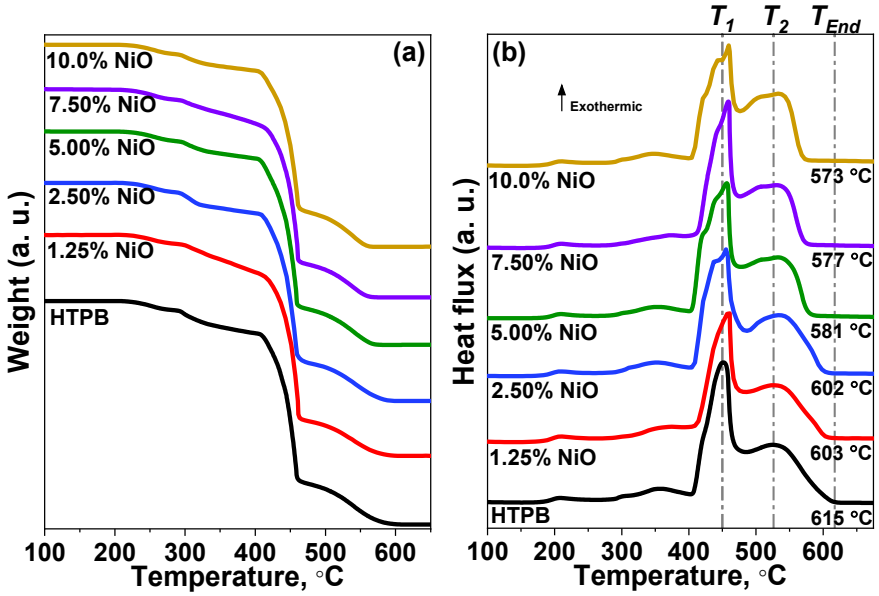

Figure 4. TG-DSC curves of the pure HTPB and NiO-loaded fuels. (**a**) TG; (**b**) DSC.

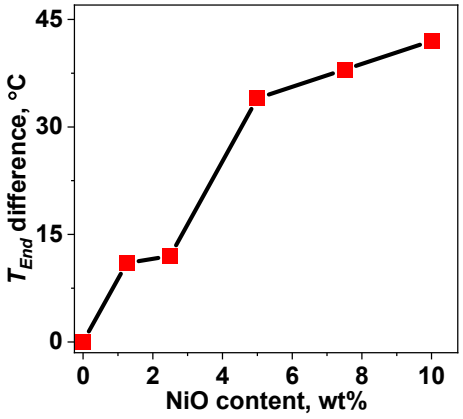

Figure 5. The end temperature difference between pure HTPB and NiO-loaded fuels.

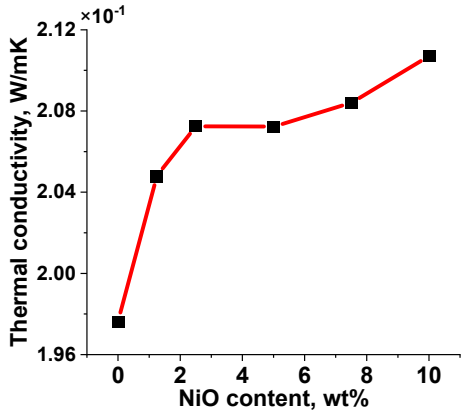

Figure 6. Thermal conductivity of the pure HTPB and NiO-loaded fuels.

Figure 7 shows the regression process of the pure HTPB and NiO-loaded fuels, where t_i represents the ignition time. Compared with the pure HTPB, the NiO-loaded fuels exhibit higher flame brightness. Combining the experimental results in Figure 7 with the thermal test results in Figure 4, the increased flame brightness in the NiO-loaded fuels originated from the catalytic effect by the NiO particles, which accelerate the pyrolysis process of the

HTPB-based fuels, hence promoting the burning process and resulting in a more intense combustion for fuel grains. Furthermore, NiO also serves as the radiating particles and improves the flame brightness of the HTPB-based fuels. The prepared fuels with a high NiO content, such as 7.50% NiO and 10.0% NiO, show a substantial increase in flame brightness relative to the pure HTPB, especially in the later stages of the burning process.

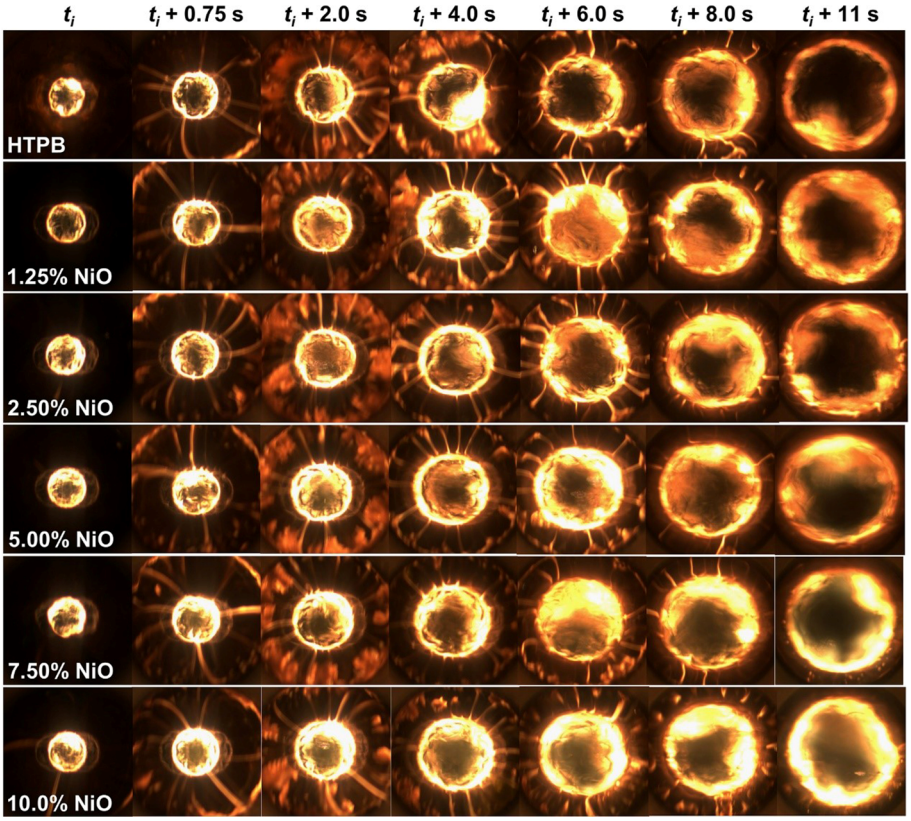

Figure 7. Regression process of the pure HTPB and NiO-loaded fuels (gaseous oxygen, 3 g/s, 1.0 MPa, the initial inner diameter of the fuel grains is 4.5 mm).

Figure 8 shows the surface features of the pure HTPB and NiO-loaded fuels after combustion termination. The 1.25% NiO, 5.00% NiO, and 10.0% NiO formulations were selected to exhibit the burning surface morphology of the NiO-loaded fuels (the fuel surface features of all NiO-loaded fuels are presented in Figure S3 of the Supplementary Materials). Compared with the pure HTPB, which shows a smooth SEM image, the loaded formulations feature an accumulation of NiO particles at the regressing surface. And this phenomenon is more obvious with the increase in NiO content. Figure 8e compares the Ni content of all formulations at the regressing surface before and after combustion, and the specific values are obtained from the energy dispersive spectrometer (EDS mapping). A linear fit is performed on the data points in Figure 8e. It is found that the slope of the fitted line for the Ni content on the regressing surface of NiO-loaded fuels is 0.1844 before combustion, while this value changed to 0.4068 after the combustion test. The above experimental results indicate that the NiO particles will gradually accumulate on the regressing surface, hence reducing the combustion surface area and inhibiting the burning process of the HTPB-based fuels. For 7.50% NiO and 10.0% NiO formulations, the above results can also be used to clarify the mechanism of the substantial increase in flame brightness when compared to the pure HTPB, especially in the later stages of the burning process (shown in Figure 7). Due to the high NiO content, the NiO residues will generate and accumulate in large quantities at the regressing surface, thereby enhancing the radiation intensity during the burning process of the fuel grains. In the later stages of the burning process, the increased diameter of the fuel grains can lead to the low velocity of the oxygen flow, making it more

difficult to blow the NiO residue away from the regressing surface, hence exacerbating the accumulation and increasing the radiation of 7.50% NiO and 10.0% NiO. In addition, the catalytic pyrolysis effects of many NiO particles on the HTPB matrix further promotes the combustion process and enhances the flame brightness.

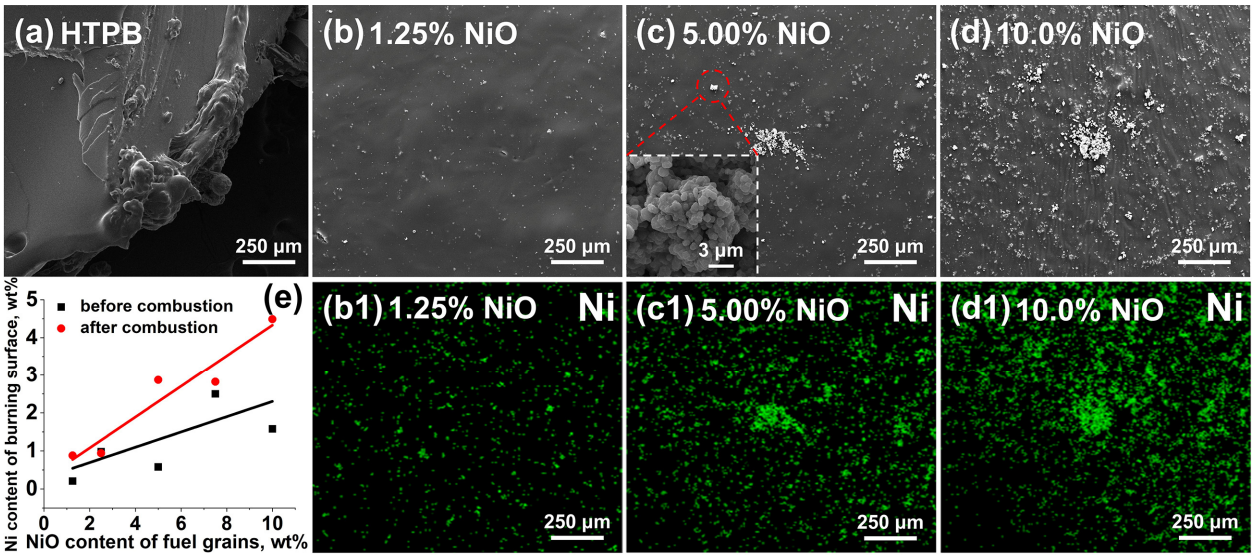

Figure 8. Fuel surface features of the pure HTPB and NiO-loaded fuels after combustion termination. (**a**–**d**) SEM images of the pure HTPB and NiO-loaded fuels; (**b1**–**d1**) EDS mapping images of NiO-loaded fuels; (**e**) Ni element content on the burning surface of NiO-loaded fuels before and after combustion.

Figure 9a shows the instantaneous regression rate vs. oxygen mass flux of pure HTPB and NiO-loaded fuels, which is obtained from the combustion images (as shown in Figure 8) and their corresponding burning surface recognition results. Each curve is the average of 3–5 runs measured under the same conditions, and the error bar represents the standard deviation of all runs. Figure 8b shows the regression rate increase of the NiO-loaded fuels, where the pure HTPB is the baseline. The detailed regression rate of all prepared fuels and the power law approximation of r_f vs. G_{ox} ($r_f = a_r \cdot G_{ox}^{n_r}$) are presented in Table 2.

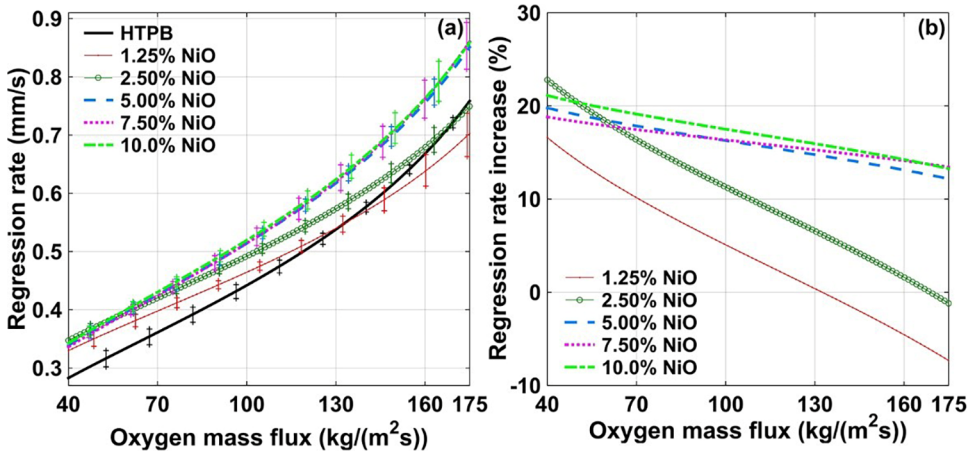

Figure 9. (**a**) Regression rate and (**b**) regression rate increase (pure HTPB is taken as the baseline) for NiO-loaded fuels.

Table 2. Regression rate and power law approximation of r_f (G_{ox}) curves for pure HTPB and NiO-loaded fuels.

	r_f (mm/s)		Δr_f (%)		$r_f = a_r\, G_{ox}^{n_r}$		R^2
G_{ox} (kg/m^{2}s)	50	150	50	150	a_r	n_r	
HTPB	0.309	0.619	-	-	0.027 ± 0.001	0.609 ± 0.001	0.985
1.25% NiO	0.353	0.601	14.2	−2.91	0.056 ± 0.001	0.465 ± 0.001	0.985
2.50% NiO	0.373	0.640	20.7	3.40	0.057 ± 0.001	0.472 ± 0.001	0.985
5.00% NiO	0.369	0.704	19.4	13.7	0.038 ± 0.001	0.568 ± 0.001	0.985
7.50% NiO	0.366	0.709	18.4	14.5	0.036 ± 0.001	0.580 ± 0.001	0.985
10.0% NiO	0.373	0.711	20.7	14.9	0.039 ± 0.001	0.567 ± 0.001	0.985

The error bars exhibited in Figure 9a are short, proving the reliability of the experimental results. Compared with pure HTPB, NiO-loaded fuels show an obvious improvement in regression rate, demonstrating the catalytic effect of NiO particles on HTPB-based fuels in the burning process. Especially in the low oxidizer mass flux, the NiO-loaded fuels exhibit a more significant regression rate increase. This result corresponds to the reduction of the n_r in NiO-loaded fuels relative to the pure HTPB, indicating that NiO particles enhance the radiative heat transfer of HTPB-based fuels on combustion [2]. When the content of NiO is lower than ($\leq$) 5 wt%, the regression rate of HTPB-based fuels increases as the NiO content increases. Nevertheless, the regression rate of the prepared fuels remains basically unchanged with the continued increase of the NiO content (5 wt% < [NiO] $\leq$ 10 wt%). Combining the characterization results in Figures 3–8, it can be deduced that the trend of the regression rate is due to the accumulation of NiO particles on the regressing surface while improving the thermal conductivity and catalyzing the pyrolysis process of the HTPB-based fuels. Since NiO particles cannot be further oxidized to release heat, the addition of NiO particles will also reduce the combustion heat of the HTPB-based fuels.

Originating from the catalysis by NiO particles on the polybutadiene component, regression rate enhancement of NiO-loaded fuels shows an obvious dependence on the additive content for NiO loads $\leq$ 5 wt%. The 5 wt% NiO particles enhance the regression rate of HTPB-based fuels by 19.4% and 13.7% at G_{ox} = 50 kg/m^{2}s and 150 kg/m^{2}s, respectively. And the higher regression rate increase in the low oxidizer mass flux (50 kg/m^{2}s) originates from the improved radiative heat transfer by the NiO particles. However, the NiO particles will also cause a reduction of combustion heat and agglomeration at the regressing surface. In the burning process of the HTPB-based fuels, the above inhibitory effects enhance linearly as the NiO content increases, while the improvement of catalytic pyrolysis effect and thermal conductivity slows down at (>) 5 wt%. Starting from the 5 wt% (5 wt% < [NiO] $\leq$ 10 wt%), more NiO particles cannot lead to a faster regression rate for HTPB-based fuels.

Detailed information about the mass burning rate is shown in Figure 10 and Table 3. Due to the high density of the NiO particles (6.84 g/cm^3 (NiO) vs. 0.93 g/cm^3 (pure HTPB)), compared with the regression rate increase, the mass burning rate increase exhibits the higher values for the NiO-loaded fuels. When the content of NiO is more than 5 wt% (5 wt% < [NiO] $\leq$ 10 wt%), the mass burning rate of HTPB-based fuels increases as the NiO content increases, which may result in a higher thrust for hybrid rocket engine. However, too much NiO also leads to a decrease in the benefit–cost ratio for the catalytic effect. At G_{ox} = 50 kg/m^{2}s, the 5 wt% NiO particles enhance the mass burning rate of HTPB-based fuels by 18.6%, while 7.5 wt% and 10.0 wt% NiO particles only increase the mass burning rate of HTPB-based fuels by 22.3% and 25.5 wt%, respectively. As mentioned in the above results and discussions, more NiO can also lead to negative effects, a reduction of combustion heat, and agglomeration at the regressing surface, worsening in a certain proportion. Therefore, there exists an optimal content of NiO in HTPB-based fuels, 5 wt%. Such a low content means that the NiO can be a suitable candidate for regression rate performance enhancement, especially in the HTPB/paraffin blends or other multi-additive HTPB composites in hybrid rocket propulsion. Small amounts of NiO particles can reduce

the content of other components or further enhance the regression rate of multi-additive HTPB composites. Furthermore, NiO contains a transition metal element, which can combine with N and O atoms on the polymer chain, and hence may enhance Young's modulus and reduce the elongation at break for fuel grains.

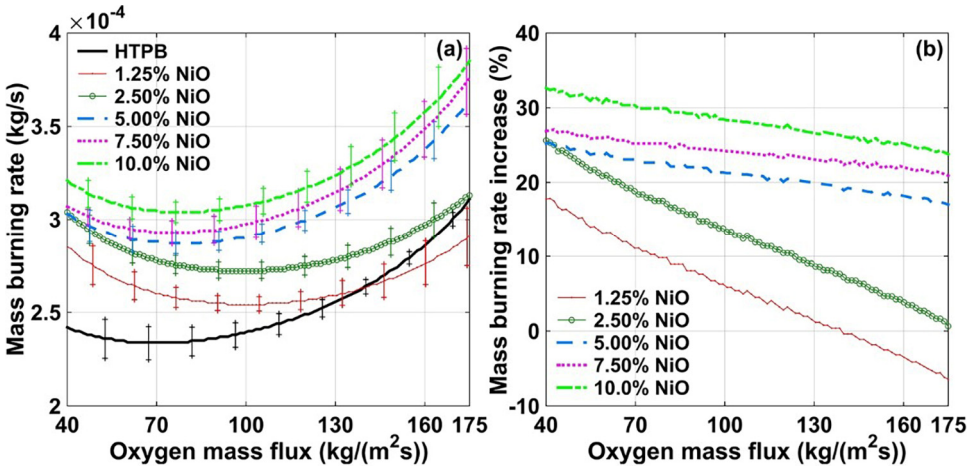

Figure 10. (**a**) Mass burning rate and (**b**) mass burning rate increase (pure HTPB is taken as the baseline) for NiO-loaded fuels.

Table 3. Mass burning rate for pure HTPB and NiO-loaded fuels.

	$m_f \times 10^4$ (mm/s)		Δm_f (%)	
G_{ox} (kg/m^{2}s)	50	150	50	150
HTPB	2.37	2.74	-	-
1.25% NiO	2.74	2.69	15.6	−1.83
2.50% NiO	2.92	2.89	23.2	5.47
5.00% NiO	2.95	3.25	24.5	18.6
7.50% NiO	3.00	3.35	26.6	22.3
10.0% NiO	3.12	3.44	31.6	25.5

4. Conclusions

This paper investigates the effects of the NiO particles on HTPB-based fuels in hybrid rocket propulsion. The presented experimental results show that NiO can intensely decrease the thermal stability of the HTPB matrix, and this catalytic effect is mainly reflected in the final pyrolysis stages of polybutadiene components. Further study indicates that NiO particles will also cause the reduction of combustion heat and the agglomeration at the regressing surface while catalyzing the pyrolysis process, improving the thermal conductivity, and promoting the radiative heat transfer of the HTPB-based fuels. Several factors lead to an optimal content of NiO in HTPB-based fuels, 5 wt%, corresponding to the regression rate increase of 19.4% and 13.7% at G_{ox} = 50 kg/m^{2}s and 150 kg/m^{2}s, respectively. This study suggests that the NiO can be a suitable candidate for regression rate performance enhancement, especially in the HTPB/paraffin blends or other multi-additive HTPB composites in hybrid rocket propulsion.

Supplementary Materials: The following supporting information can be downloaded at: https://www.mdpi.com/article/10.3390/aerospace10090800/s1, Figure S1: The physical picture of the 2D-radial hybrid burner [31]; Figure S2: The surface morphology of the NiO loaded fuels; Figure S3: Fuel surface features of the NiO loaded fuels after combustion termination; Table S1: Thermal conductivity of the pure HTPB and NiO loaded fuels.

Author Contributions: Conceptualization, R.S. and H.Y.; Methodology, H.Y.; Software, L.T.D.; Validation, H.Y., X.Y., H.G. and W.Z.; Formal Analysis, H.Y.; Investigation, H.Y.; Resources, R.S.; Data Curation, H.Y.; Writing—Original Draft Preparation, H.Y.; Writing—Review and Editing, H.Y., X.Y., H.G., L.T.D., W.Z. and R.S.; Visualization, H.Y.; Supervision, R.S.; Project Administration, W.Z.; Funding Acquisition, W.Z. All authors have read and agreed to the published version of the manuscript.

Funding: This work was supported by the National Natural Science Foundation of China (Grant No. 12074187).

Data Availability Statement: Not applicable.

Conflicts of Interest: The authors declare no conflict of interest.

References

1. Chiaverini, M.J. *Hybrid Propulsion, Encyclopedia of Aerospace Engineering*; John Wiley & Sons, Ltd.: Hoboken, NJ, USA, 2010. [CrossRef]
2. Chiaverini, M.J.; Kuo, K.K. *Fundamentals of Hybrid Rocket Combustion and Propulsion*; American Institute of Aeronautics and Astronautics: Reston, VA, USA, 2007. [CrossRef]
3. John, J.; Nandagopalan, P.; Baek, S.W.; Miglani, A. Rheology of solid-like ethanol fuel for hybrid rockets: Effect of type and concentration of gellants. *Fuel* **2017**, *209*, 96–108. [CrossRef]
4. Jeong, J.; Bhosale, V.K.; Kwon, S. Ultrafast igniting, low toxicity hypergolic hybrid solid fuels and hydrogen peroxide oxidizer. *Fuel* **2021**, *286*, 119307. [CrossRef]
5. Bhosale, V.K.; Jeong, J.; Kwon, S. Ignition of boron-based green hypergolic fuels with hydrogen peroxide. *Fuel* **2019**, *255*, 115729. [CrossRef]
6. Mazzetti, A.; Merotto, L.; Pinarello, G. Paraffin-based hybrid rocket engines applications: A review and a market perspective. *Acta Astronaut.* **2016**, *126*, 286–297. [CrossRef]
7. Merotto, L.; Galfetti, L.; Colombo, G.; DeLuca, L. Characterization of nAl powders for rocket propulsion. *Prog. Propuls. Phys. (EUCASS)* **2011**, *2*, 99–120. [CrossRef]
8. Zhang, Q.; Shu, Y.; Liu, N.; Lu, X.; Shu, Y.; Wang, X.; Mo, H.; Xu, M. Hydroxyl terminated polybutadiene: Chemical modification and application of these modifiers in propellants and explosives. *Cent. Eur. J. Energetic Mater.* **2019**, *16*, 153–193. [CrossRef]
9. Aoki, A.; Fukuchi, A.B. Development of low cost fuels for hybrid rocket engine. In Proceedings of the 46th AIAA/ASME/SAE/ASEE Joint Propulsion Conference & Exhibit, Nashville, TN, USA, 25–28 July 2010; p. 6638. [CrossRef]
10. Zhou, Q.; Jie, S.; Li, B.C. Preparation of hydroxyl-terminated polybutadiene with high cis-1,4 content. *Ind. Eng. Chem. Res.* **2014**, *53*, 17884–17893. [CrossRef]
11. Dennis, C.; Bojko, B. On the combustion of heterogeneous AP/HTPB composite propellants: A review. *Fuel* **2019**, *254*, 115646. [CrossRef]
12. Sun, X.; Tian, H.; Li, Y.; Yu, N.; Cai, G. Regression rate behaviors of HTPB-based propellant combinations for hybrid rocket motor. *Acta Astronaut.* **2016**, *119*, 137–146. [CrossRef]
13. Sutton, G.P.; Biblarz, O. *Rocket Propulsion Elements*; John Wiley & Sons: Hoboken, NJ, USA, 2016.
14. Deluca, L.T.; Shimada; Sinditskii, V.P.; Calabro, M. *Chemical Rocket Propulsion: A Comprehensive Survey of Energetic Materials*; Springer Aerospace Technology: Berlin, Germany, 2016.
15. Marothiya, G.; Kumar, R.; Ramakrishna, P.A. Enhancing the regression rate of hydroxyl-terminated-polybutadiene-based mixed hybrid rockets. *J. Propuls. Power* **2022**, *38*, 623–630. [CrossRef]
16. Lee, D.; Lee, C. AP and Boron combustion characteristics in staged hybrid rocket engine. In Proceedings of the 52nd AIAA/SAE/ASEE Joint Propulsion Conference, Salt Lake City, UT, USA, 25–27 July 2016. [CrossRef]
17. Hori, K.; Wada, Y.; Hasegawa, K.; Yagishita, T.; Kobayashi, K.; Iwasaki, S.; Sato, H.; Nishioka, M.; Kimura, M. Combustion characteristics of hybrid rocket motor using GAP as a solid fuel (II). In Proceedings of the 47th AIAA/ASME/SAE/ASEE Joint Propulsion Conference & Exhibit, San Diego, CA, USA, 31 July–3 August 2011. [CrossRef]
18. Frederick, J.R.A.; Whitehead, J.J.; Knox, L.R.; Moser, M.D. Regression rates study of mixed hybrid propellants. *J. Propuls. Power* **2007**, *23*, 175–180. [CrossRef]
19. Chen, S.; Tang, Y.; Yu, H.; Bao, L.; Zhang, W.; DeLuca, L.T.; Shen, R.; Ye, Y. The rapid H_2 release from AlH_3 dehydrogenation forming porous layer in AlH_3/hydroxyl-terminated polybutadiene (HTPB) fuels during combustion. *J. Hazard. Mater.* **2019**, *371*, 53–61. [CrossRef]
20. Wu, Y.; Zhang, Z.; Wang, Q.; Wang, N. Combustion characteristics of skeleton polymer reinforced paraffin-wax fuel grain for applications in hybrid rocket motors. *Combust. Flame* **2022**, *241*, 112055. [CrossRef]
21. Armold, D.M. *Formulation and Characterization of Paraffin-Based Solid Fuels Containing Swirl Inducing Grain Geometry and/or Energetic Additives*; Statechurch; The Pennsylvania State University: State College, PA, USA, 2014.
22. Zhang, S.; Hu, F.; Zhang, W. Numerical investigation on the regression rate of hybrid rocket motor with star swirl fuel grain. *Acta Astronaut.* **2016**, *127*, 384–393. [CrossRef]

23. Thomas, J.C.; Stahl, J.M.; Tykol, A.J.; Rodriguez, F.A.; Peterson, E.L. Hybrid rocket studies using HTPB/paraffin fuel blends in gaseous oxygen flow. In Proceedings of the 7th European Conference for Aeronautics and Space Sciences (EUCASS), Milan, Italy, 3–6 July 2015. [CrossRef]
24. Dunn, C.; Gustafson, G.; Edwards, J.; Dunbrack, T.; Johansen, C. Spatially and temporally resolved regression rate measurements for the combustion of paraffin wax for hybrid rocket motor applications. *Aerosp. Sci. Technol.* **2018**, *72*, 371–379. [CrossRef]
25. Yu, H.; Shen, R.; Tang, Y.; Chen, S.; DeLuca, L.T.; Zhang, W.; Ye, Y.H. The verifications and demonstrations of self-disintegration fuel concept for hybrid propulsion. In Proceedings of the 8th European Conference For Aeronautics And Space Sciences, Madrid, Spain, 1–4 July 2019. [CrossRef]
26. Yu, X.; Yu, H.; Zhang, W.; DeLuca, L.T.; Shen, R. Effect of Penetrative Combustion on Regression Rate of 3D Printed Hybrid Rocket Fuel. *Aerospace* **2022**, *9*, 696. [CrossRef]
27. Varfolomeev, M.A.; Yuan, C.; Bolotov, A.V.; Minkhanov, I.F.; Mehrabi-Kalajahi, S.; Saifullin, E.R.; Marvanov, M.M.; Baygildin, E.R.; Sabiryanov, R.M.; Rojas, A.; et al. Effect of copper stearate as catalysts on the performance of in-situ combustion process for heavy oil recovery and upgrading. *J. Pet. Sci. Eng.* **2021**, *207*, 109125. [CrossRef]
28. Moroi, G. Influence of ion species on the thermal degradation of polyurethane interaction products with transition metal ions. *J. Anal. Appl. Pyrolysis* **2004**, *71*, 485–500. [CrossRef]
29. Pal, Y.; Mahottamananda, S.N.; S, S.; Palateerdham, S.K.; Ingenito, A. Thermal decomposition kinetics and combustion performance of paraffin-based fuel in the presence of CeO_2 catalyst. *Firephyschem* **2023**, *3*, 217–226. [CrossRef]
30. Cardoso, K.P.; Ferrão, L.F.A.; Kawachi, E.Y.; Gomes, J.S.; Nagamachi, M.Y. Ballistic Performance of Paraffin-Based Solid Fuels Enhanced by Catalytic Polymer Degradation. *J. Propuls. Power* **2019**, *35*, 115–124. [CrossRef]
31. Yu, H.; Chen, S.; Yu, X.; Zhang, W.; Paravan, C.; DeLuca, L.T.; Shen, R. Nickel acetylacetonate as decomposition catalyst for HTPB-based fuels: Regression rate enhancement effects. *Fuel* **2021**, *305*, 121539. [CrossRef]
32. Yu, H.; Yu, X.; Chen, S.; Zhang, W.; DeLuca, L.T.; Shen, R. The catalysis effects of acetylacetone complexes on polymer matrix of HTPB-based fuels. *Firephyschem* **2021**, *1*, 205–211. [CrossRef]
33. Paravan, C. Nano-sized and mechanically activated composites: Perspectives for enhanced mass burning rate in aluminized solid fuels for hybrid rocket propulsion. *Aerospace* **2019**, *6*, 127. [CrossRef]
34. Ye, Y.; Shu, L.; Shen, R. Effect of phenolic resin on laser ablation of B/KNO_3. *Chin. J. Energetic Mater.* **2007**, *19*, 68–77. [CrossRef]
35. Chen, S.; Tang, Y.; Yu, H.; Guan, X.; DeLuca, L.T.; Zhang, W.; Shen, R.; Ye, Y. Combustion enhancement of hydroxyl-terminated polybutadiene by doping multiwall carbon nanotubes. *Carbon* **2019**, *144*, 472–480. [CrossRef]